

Article

Efficient Utilization of Hydrocarbon Mixture to Produce Aromatics over Zn/ZSM-5 and Physically Mixed with ZSM-5

Hyunjin Shim, Jinju Hong  and Kyoung-Su Ha *

Department of Chemical and Biomolecular Engineering, Sogang University, 35 Baekbeom-ro, Mapo-gu, Seoul 04107, Korea; hjinsim@sogang.ac.kr (H.S.); pearlhong@sogang.ac.kr (J.H.)

* Correspondence: philoseus@sogang.ac.kr

Abstract: A mixture of saturated and unsaturated light hydrocarbon was used as feed gas for the production of aromatics. Natural gas liquids (NGL) from gas fields and hydrocarbon molecules obtained in the middle of conversion processes could be considered a kind of light hydrocarbon mixture. Therefore, for the conversion of the mixture into aromatics compounds, Zn-impregnated ZSM-5 catalysts were prepared and evaluated by employing different loading of Zn. In addition, the catalytic performance was tested and compared by charging physically mixed two different kinds of catalysts in the bed. The NH₃-TPD result showed that the impregnation of Zn led to an increase in the number of medium-strength acid sites, whereas those of weak and strong acid sites were decreased. From the results of the catalytic activity tests, 0.5Zn/ZSM-5 showed the highest aromatics yield. As the amount of Zn loading was further increased to 1 wt.%, the yield of aromatics decreased. The test result in the case of the physically mixed catalysts showed a slightly lower yield in terms of total aromatics, but showed the highest BTX yield. To reveal the relative contribution of each hydrocarbon conversion to aromatics yield, each C₂ compound was separately tested for aromatization over Zn/ZSM-5.

Keywords: aromatization; light hydrocarbon; ZSM-5 zeolite; Zn; acid site



Citation: Shim, H.; Hong, J.; Ha, K.-S. Efficient Utilization of Hydrocarbon Mixture to Produce Aromatics over Zn/ZSM-5 and Physically Mixed with ZSM-5. *Catalysts* **2022**, *12*, 501. <https://doi.org/10.3390/catal12050501>

Academic Editor: Francis Verpoort

Received: 28 March 2022

Accepted: 27 April 2022

Published: 29 April 2022

Publisher's Note: MDPI stays neutral with regard to jurisdictional claims in published maps and institutional affiliations.



Copyright: © 2022 by the authors. Licensee MDPI, Basel, Switzerland. This article is an open access article distributed under the terms and conditions of the Creative Commons Attribution (CC BY) license (<https://creativecommons.org/licenses/by/4.0/>).

1. Introduction

There have been many approaches to convert methane into versatile high-value-added chemicals through harnessing and utilizing large amounts of natural gas reservoirs, including shale gas, biogas, waste gas, and so on [1–3]. Direct conversion of methane into final products such as ethylene, benzene, toluene, xylenes, and other aromatic compounds seems very innovative and economical considering the shortened reaction pathway and more simplified process schemes having a smaller number of treatment steps. There have been several representative examples of this direct conversion of methane, such as methane dehydroaromatization (MDA) [4], oxidative coupling of methane (OCM) [5], and the DICP-developed method using an Fe-based single-site catalyst [6]. Regarding the production of aromatics through the MDA method, the best yield of BTX aromatics was reported as about 20% [7,8], and mostly benzene was formed. In addition, the catalyst usually deactivates due to severe coke formation, which requires periodic or continuous regeneration of the catalyst bed. The DICP-developed catalyst has been known to show very stable performance, yielding ethylene, hydrogen, benzene, and naphthalene at high selectivity. Despite the catalytic performance and stability, the preparation of the catalyst seems difficult due to its very high temperature of around 1700 °C, and it also seems relatively difficult to assess because the catalyst should be prepared with single-atom active sites in the form of Si-Fe-C, according to the literature [6]. Unfortunately, those methods require sophisticated and complicated catalysts that are difficult to prepare, and a very high temperature to activate reactants, both of which may limit a possibility of commercialization. Due to this limitation, recent studies have turned their attention to more

energy-efficient ways under less harsh conditions, even though the process is composed of several treatment steps. The traditional approach is a well-known indirect method via synthesis gas; it is composed of a synthesis-gas-generation step and additional synthesis steps such as Fischer–Tropsch synthesis, methanol synthesis, dimethyl ether synthesis, and so on. However, the replacement of the first step with more recently developed plasma-assisted reforming methods innovated the traditional indirect processes by lowering the energy requirement and reducing greenhouse gases [9–15]. The low-temperature plasma-assisted reforming under nonthermal equilibrium is characterized by low temperature, a lower energy requirement, additional products besides syngas, etc. This nonthermal plasma method can be applied to the above-mentioned methods such as MDA and make it a two-step process. We have tried to convert methane into hydrocarbon intermediates in order to more easily convert them further into aromatic compounds. After a series of tests, the hydrocarbon intermediates from the low-temperature plasma-assisted conversion of methane could be identified as a mixture composed of saturated and unsaturated light hydrocarbon and hydrogen as shown in Table 1. To utilize this mixture as it is without energy-intensive gas-separation steps, a multifunctional catalyst having at least two active sites for saturated and unsaturated hydrocarbon seems necessary so that as much of the mixture as possible can be converted into aromatic products. Regarding MDA reaction, the necessary active sites for converting methane into aromatics were identified as metal carbide such as Mo_2C for methane coupling, and the Brønsted acid site of zeolite for cyclization of the intermediates [2,16]. For the conversion of C_{2+} , various metal components were tested and reported elsewhere [17–19]. For the conversion of C_3 and C_4 , Ga and Mo were known to be active [20–24], whereas Zn was more effective for the conversion of C_2 [25,26].

Table 1. Feed gas composition.

Component	Vol. %
H_2	36.70
C_2H_2	7.50
C_2H_4	1.13
C_2H_6	1.67
C_3H_8	0.803
n- C_4H_{10}	2.06
N_2	50.137

In this study, we focus on the catalytic conversion of this mixture into value-added aromatic compounds and also investigate the effects of Zn-derived active sites and conventional acid sites from H-form ZSM-5 zeolite on the performance and deactivation.

2. Results

2.1. Catalyst Characterization

Figure S1 shows the XRD patterns of the prepared Zn-impregnated ZSM-5 catalysts and ZSM-5 exhibited MFI-type structure. The diffraction peaks at 7.9, 8.8, 9.0, 23.0, 23.2, 23.7, 23.9, and 24.4° were clearly observed, corresponding to (1 0 1), (0 2 0), (1 1 1), (3 3 2), (0 5 1), (1 5 1), (3 0 3), and (1 3 3) reflection planes, respectively [27]. The characteristic peaks of crystalline ZnO particles were not observed, which indicated that the incorporated Zn species were so finely dispersed that agglomerated bulk phase of ZnO located outside the pores might not be generated [27,28]. Figure 1 shows the images of SEM-EDS analysis, corroborating that the Zn species were well-dispersed.

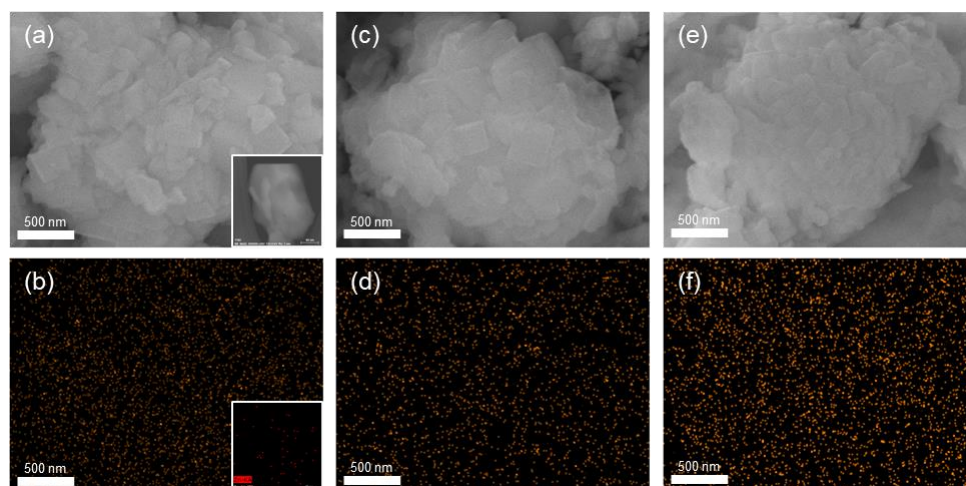


Figure 1. SEM image and corresponding energy-dispersive spectroscopy (EDS) mapping of Zn (a,b) 0.25Zn/ZSM-5; inset: TEM image and EDS mapping of Zn, (c,d) 0.5Zn/ZSM-5 and (e,f) 1Zn/ZSM-5.

The isotherm of the samples from N_2 physisorption are shown in Figure S2. The isotherm confirms the microporous character of the ZSM-5 catalysts. Since the amount of impregnated Zn was little, Zn-impregnation did not lead to significant difference in the adsorbed amount of N_2 . Table 2 shows the amount of Zn loading and Si/Al ratio determined by ICP-OES and the textural properties of the samples measured by physisorption. The ICP-OES result confirmed that the amount of Zn loading and Si/Al ratio of the samples coincided well with the prescribed values in the name of each catalyst. The Zn loading did not change the textural properties of the catalyst very much. When 1 wt.% of Zn was impregnated, S_{BET} slightly decreased. In addition, as the amount of impregnated Zn increased, S_{ext} slightly increased.

Table 2. Zn loading and Si/Al ratio determined by ICP-OES analysis and textural properties of the catalysts determined by N_2 physisorption analysis.

Catalysts	Zn Loading (wt.%) ^a	Si/Al Ratio ^a	S_{BET} ($m^2 g^{-1}$)	S_{ext} ^b ($m^2 \cdot g^{-1}$)	V_{total} ^c ($cm^3 \cdot g^{-1}$)	V_{micro} ^d ($cm^3 \cdot g^{-1}$)
ZSM-5	-	17.0	377.2	29.0	0.17	0.15
0.25Zn/ZSM-5	0.23	16.5	378.3	29.4	0.21	0.15
0.5Zn/ZSM-5	0.49	16.9	377.0	29.7	0.18	0.15
1Zn/ZSM-5	1.01	16.7	362.6	30.9	0.19	0.15

Notation: S_{BET} : Brunauer–Emmett–Teller (BET) surface area, S_{ext} : external surface area, V_{total} : total pore volume, V_{micro} : micropore volume. ^a determined by ICP-OES analysis. ^b calculated by *t*-plot method. ^c calculated by DFT method. ^d calculated by H-K method.

The acidic properties of the prepared catalysts analyzed by the NH_3 -TPD. NH_3 -TPD profile with deconvoluted subpeaks are shown in Figure 2. The acidity of each acid site calculated from deconvolution and each ratio are shown in Table 3. Unimpregnated ZSM-5 showed large quantities of weak and strong acid sites, whereas that of medium-strength acid sites was found to be relatively small. In contrast, Zn/ZSM-5 was shown to have a relatively decreased number of weak acid sites, whereas the number of strong acid sites reached its maximum at 0.25Zn/ZSM-5, but those of the other impregnated catalysts showed relatively smaller quantities of strong acid sites. The number of medium acid sites was greatly increased when Zn was incorporated, but they decreased as the loading of Zn increased. This effect of Zn impregnation seemed to be attributed to the interaction between acidity of ZSM-5 and the incorporated Zn species, which was known to produce Zn-associated Lewis acid sites, most of which could be regarded as medium-strength acid sites. These Zn-associated acid sites are considered active sites for the light alkane

dehydrogenation [29–35]. Regarding the total acidity, the amount decreased as Zn loading increased. This seemed to be ascribed to the coverage of acid sites by incorporation of Zn [28,36].

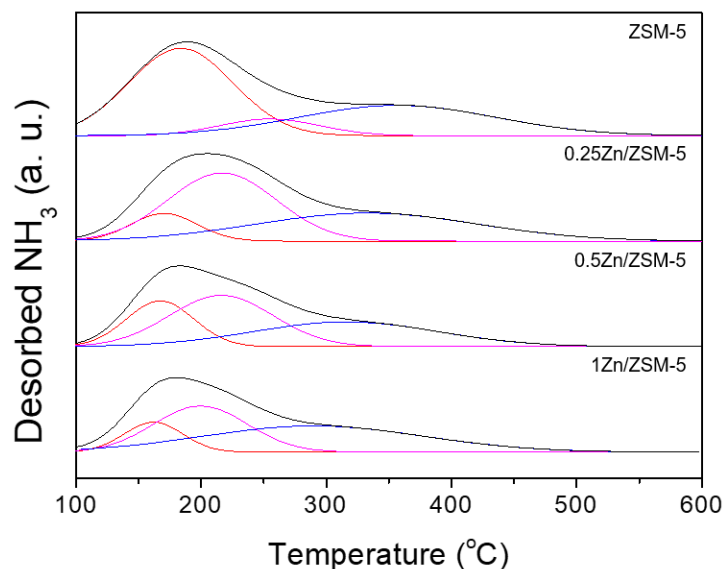


Figure 2. NH₃-TPD results of ZSM-5, 0.25Zn/ZSM-5, 0.5Zn/ZSM-5 and 1Zn/ZSM-5.

Table 3. Acidity of the catalysts.

Catalysts	Acidity (mmol-NH ₃ /g _{cat}) ^a			
	Weak	Medium	Strong	Total Acidity
ZSM-5	0.505 (54%)	0.091 (10%)	0.331 (36%)	0.928
0.25Zn/ZSM-5	0.103 (12%)	0.410 (48%)	0.345 (40%)	0.858
0.5Zn/ZSM-5	0.171 (24%)	0.296 (41%)	0.254 (35%)	0.720
1Zn/ZSM-5	0.098 (15%)	0.241 (36%)	0.321 (49%)	0.659

^a calculated from peak area of NH₃-TPD profiles.

XPS analysis was conducted to study the state of Zn species incorporated into the zeolite. Zn 2p 3/2 spectra were shown in Figure 3 and two Zn species could be assigned in this figure. ZnO species could be assigned to the lower binding energies of 1022.9–1023.2 eV and higher binding energies around 1025.1–1025.6 eV could be assigned to [Zn-O-Zn]²⁺ species exhibiting Lewis acidity formed by the interaction between acid sites of ZSM-5 and the incorporated Zn species [27,37,38]. Careful observation revealed that 0.25Zn/ZSM-5 had more amount of [Zn-O-Zn]²⁺ species than that of ZnO. The amount of [Zn-O-Zn]²⁺ in the case of 0.5Zn/ZSM-5 was slightly smaller, but the amount of ZnO was much greater than that in the case of 0.25Zn/ZSM-5. 1Zn/ZSM-5 was found to show that the ZnO phase seemed dominant compared with those of other impregnated catalysts. From this observation, incorporation in the form of ZnO appeared more favorable when a greater amount of Zn loading was applied. From references, the [Zn-O-Zn]²⁺ site was identified as a Lewis acid site and believed to be the medium acid site. The observation of XPS that the composition of the medium acid site was the highest at 0.25Zn/ZSM-5 and the number of medium acid sites decreased as Zn loading increased coincided well with the result of NH₃-TPD in Figure 2.

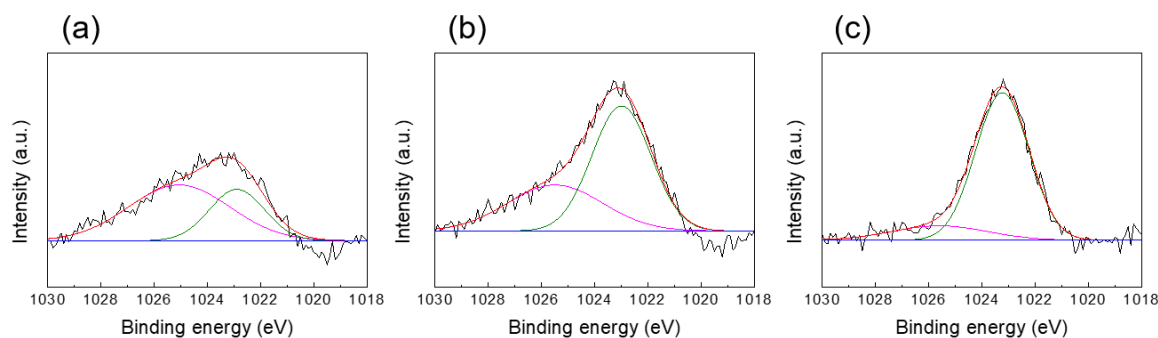


Figure 3. Zn 2P 3/2 XPS spectra of fresh (a) 0.25Zn/ZSM-5, (b) 0.5Zn/ZSM-5 and (c) 1Zn/ZSM-5.

2.2. Catalytic Activity Tests

The total carbon conversion and selectivity of produced aromatics were shown in Figure 4 and more detailed performance result at TOS 10 and 50 min was given in Table 4. The total carbon conversion did not show appreciable difference among the catalysts, whereas 0.5Zn/ZSM-5 showed the highest aromatics yield. When the amount of Zn loading was further increased to 1 wt.%, it resulted in lower catalytic activity in terms of aromatics yield than that of ZSM-5. In terms of the surface area and the distribution of acid sites, 1 wt.% of Zn incorporation seemed to exert negative effects on the structure of ZSM-5 and the catalyst showed lower acidity and lower catalytic performance as well. This result indicated that enhancing catalytic performance through Zn incorporation seemed to have a certain optimum point. From the results of NH₃-TPD analysis, Zn impregnation led to decreased weak and strong acidity and the total acidity was decreased.

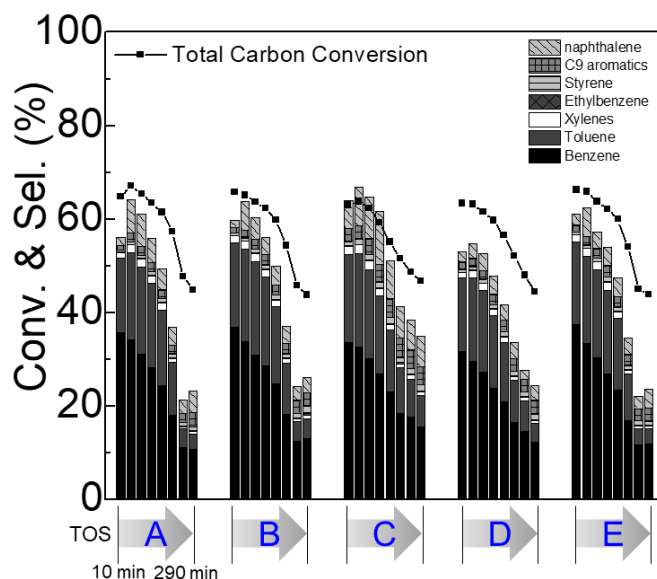


Figure 4. Total carbon conversion and aromatics selectivity of A: ZSM-5, B: 0.25Zn/ZSM-5, C: 0.5Zn/ZSM-5, D: 1Zn/ZSM-5, and E: ZSM-5 + 0.5Zn/ZSM-5.

Table 4. Total carbon conversion, selectivity, and yield of aromatics at TOS 10 and 50 min.

Catalysts	TOS (min)	Total Carbon Conversion (%)	Aromatics Selectivity (%)							BTX Yield (%)	Total Aromatics Yield (%)
			Benzene	Toluene	Xylenes	EtBz	Styrene	C ₉	C ₁₀		
ZSM-5	10	64.8	35.7	15.9	1.32	0.07	0.44	0.94	1.77	41.8	44.4
	50	67.1	34.3	18.6	1.64	0.09	0.57	1.87	7.16	43.6	51.4
0.25Zn/ZSM-5	10	65.7	36.9	18.1	1.47	0.08	0.56	1.21	1.39	44.7	47.3
	50	65.1	33.9	19.7	1.67	0.10	0.64	1.71	6.06	43.8	50.6
0.5Zn/ZSM-5	10	63.0	33.6	18.9	1.78	0.11	0.93	2.74	6.01	42.3	49.9
	50	63.8	32.6	20.0	1.83	0.15	1.10	2.85	8.34	42.9	52.8
1Zn/ZSM-5	10	63.4	31.7	15.9	1.09	0.07	0.53	1.67	2.10	38.5	42.0
	50	63.2	29.5	18.0	1.47	0.11	0.75	1.79	3.11	38.8	43.4
ZSM-5 + 0.5Zn/ZSM-5	10	66.3	37.5	17.7	1.47	0.08	0.56	1.40	2.45	44.8	48.3
	50	65.9	33.3	18.8	1.61	0.10	0.62	1.90	6.13	42.8	49.7

In order to keep the proper amount of acid sites, unimpregnated ZSM-5 was physically mixed with 0.5Zn/ZSM-5. The performance result of this physically mixed catalyst bed showed a slightly lower yield in terms of total aromatics compared with the result of 0.5Zn/ZSM-5. Interestingly, the physically mixed catalyst showed the highest BTX yield, but C₉ (1,2,4-trimethylbenzene) and C₁₀ (naphthalene) aromatic compounds considered coke precursors were relatively less produced [39] in comparison with 0.5Zn/ZSM-5 and 1Zn/ZSM-5 catalysts, as shown in Table 4. From this finding, we tried another catalytic test with 0.25 wt.% Zn loading, which is an equivalent amount of Zn in the physically mixed bed. As shown in Figure 4, the conversion was slightly decreased but BTX and total aromatics yields were very similar to those of the physically mixed bed. From this comparison, it seemed that BTX yield could be maximized and aromatic coke precursors minimized at the same time with highly dispersed Zn species in ZSM-5, which could be obtained by limiting the Zn loading to less than 0.5 wt.%. In addition, Zn incorporation into ZSM-5 led to different reaction pathways toward aromatics formation. In the case of unimpregnated ZSM-5, the large amount of total acidity, especially Brønsted acid sites, played roles in cracking and cyclization. On the other hand, the Zn-impregnated ZSM-5 had an additional kind of [Zn-O-Zn]²⁺ sites, different from Brønsted acid sites. The [Zn-O-Zn]²⁺ sites facilitated the formation of dehydrogenated intermediates that could further generate alkylated aromatics, as confirmed in Figure 4 and Table 4.

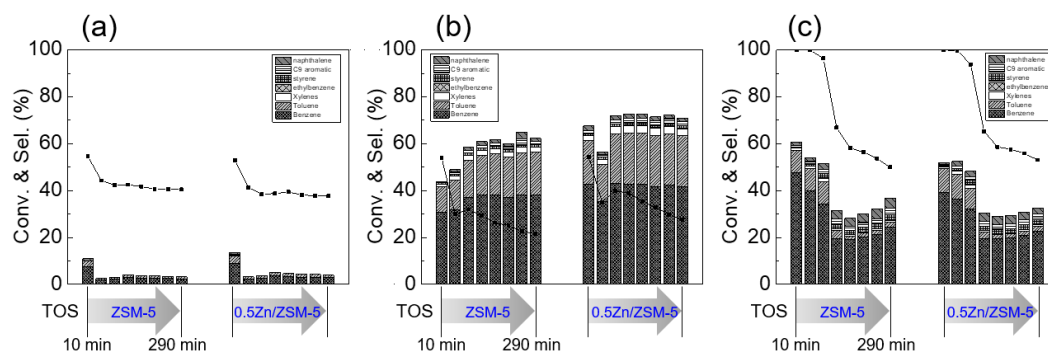
Besides aromatics, aliphatic hydrocarbons were also produced during reaction and the selectivities were given in Figure S4. The TG/DTA result of the spent catalysts is given in Figure S5. All the spent catalysts experienced weight loss above 600 °C, indicating that graphitic coke species were mainly formed and responsible for deactivation.

Table 5 showed the conversion of each reactant species in the hydrocarbon mixture. C₂H₂ and n-C₄H₁₀ exhibited almost a full conversion. C₃H₈ showed a very high conversion over 86%, and most exceeded 90%. C₂H₆ and C₂H₄, however, showed negative conversions throughout the reaction time. This indicates that C₂H₆ and C₂H₄ were produced rather than consumed, since the higher reactivity of acetylene led to more hydrogenated C₂ species and a series of cracking and dehydrogenation of C₃-C₄ took place [40–43]. The lowest amounts of C₂H₆ and C₂H₄ were produced when physically mixed catalyst was used, indicating that utilization of C₂H₆ and C₂H₄ were relatively preferred. Physically mixed catalyst bed showed the highest amount of produced H₂ at a TOS of 10 min.

Table 5. The conversion of each reactant gas observed at TOS 10 and 50 min.

Catalysts	TOS (min)	Conversion (%)					
		H ₂	C ₂ H ₆	C ₂ H ₄	C ₂ H ₂	C ₃ H ₈	n-C ₄ H ₁₀
ZSM-5	10	-14.7	-28.1	-124.6	99.9	97.2	100
	50	-3.84	-24.8	-121.2	99.9	95.3	100
0.25Zn/ZSM-5	10	-10.6	-25.3	-121.7	99.9	97.2	100
	50	-3.43	-25.9	-129.0	99.9	94.1	100
0.5Zn/ZSM-5	10	-12.6	-22.5	-137.5	99.9	93.1	99.7
	50	-1.33	-27.2	-139.2	99.8	86.9	99.0
1Zn/ZSM-5	10	-7.33	-37.0	-133.6	99.9	97.2	100
	50	-1.54	-32.5	-144.5	99.8	90.5	100
ZSM-5 + 0.5Zn/ZSM-5	10	-16.6	-21.8	-116.7	99.9	97.5	100
	50	-2.89	-24.4	-126.3	99.9	94.7	100

To further investigate the role of incorporated Zn species, ethane, ethylene and acetylene were used as a sole hydrocarbon reactant, respectively, and a catalytic activity test for each species was conducted and the test result is shown in Figure 5. In each case, conversion of each species did not change a lot, but the selectivity seemed to vary. In the case of ethane conversion in Figure 5a, the highest aromatics yields from ZSM-5 and 0.5Zn/ZSM-5 were measured as 5.94% and 7.17%, respectively, indicating Zn-incorporated Lewis acid sites contributed to formation of ethylenic compounds and ultimately aromatics. It was noteworthy that the highest yield of aromatics over Zn-impregnated ZSM-5 had considerably increased up to 36.7% when compared with that of ZSM-5 (23.5%) in the case of ethylene feed.

**Figure 5.** Catalytic performance of ZSM-5 and 0.5Zn/ZSM-5 when (a) ethane, (b) ethylene, and (c) acetylene was used as reactant.

According to the dehydrogenation mechanism of ethane over Zn-associated Lewis acid sites [25,26,44,45], C₂H₆ is first deprotonated to C₂H₅⁺ over Zn-Lewis acid sites. Then, dehydrogenation could be completed by further deprotonation of C₂H₅⁺ combined with reaction with a nearby Brønsted acid site that yields C₂H₄ and H₂. Ethylene was believed to be one of the most important intermediates for aromatization synthesis, and Brønsted acid sites present in zeolite were mainly regarded as active sites for aromatization of ethylene [2]. Toluene and xylenes could be produced by cyclotrimerization of ethylene with further alkylation. Isomerization and disproportionation of reactant and products could also lead to the formation of other aromatic species [46–48]. In the H₂-rich environment as in our study, aromatization of ethylene at Brønsted acid sites mentioned above could be retarded by hydrogenation of ethylene. The incorporated Zn species in ZSM-5, however, seemed to facilitate aromatization of ethylene by suppressing hydrogenation to some extent. Looking into the selectivity of each component in Figure 5b, those of benzene, toluene, and xylenes were greatly improved in the case of 0.5Zn/ZSM-5.

According to the mechanism of acetylene aromatization proposed by Tsai et al [49], acetylene could react with the Brønsted acid site present in zeolite generating $C_2H_3^+$. Then, further react with acetylene and $C_2H_3^+$ followed by successive oligomerization, which could yield aromatic compounds with the help of zeolitic shape selectivity. From this perspective, the decreased number of aromatics yielded by employing 0.5Zn/ZSM-5 could be ascribed to the decreased number of acid sites as shown in the previous NH_3 -TPD result. As shown in Figure 5c, benzene was far more synthesized over ZSM-5 among other products at early stage (10–90 min) than in the case of 0.5Zn/ZSM-5.

As a result of combining the effect of aromatization from saturated and unsaturated hydrocarbons under an H_2 -rich environment, the highest yield of total aromatics was obtained in the case of 0.5Zn/ZSM-5, while the highest yield of BTX was obtained in the cases of physically mixed catalytic bed and 0.25Zn/ZSM-5, which seemed comparable.

2.3. Remarks about Utilization of Methane as A Primary Component of Natural Gas, Including Shale Gas

Regarding harnessing methane as a carbon resource to synthesize aromatics, we are now showing how much methane was possible to be converted and how many aromatics, including BTX, were generated on the basis of lab-scale experiments. These may not be commercially meaningful numbers at present, but we can consider this result to have potential for the 2-step approach. For the conversion of methane as a first step, we took an example of nonthermal plasma-assisted reaction system in the previous section [15]. Considering Table S1 showing intermediate hydrocarbon compositions from the plasma-assisted conversion of methane, feed mixture for aromatization of this study was given in Table 1. Using this, the aromatics yield from methane is shown in Table 6. The potential maximum yields of BTX and total aromatics from methane were estimated as 23.7% (physically mixed bed) and 28.0% (0.5Zn/ZSM-5), respectively.

Table 6. Methane conversion and aromatics yield in a 2-step process composed of plasma reactor followed by catalytic aromatization over Zn/ZSM-5.

DBD Plasma	Catalytic Aromatization of Light Hydrocarbons			Methane-to-BTX Yield (%)	Methane-to-Aromatics Yield (%)
	Methane Conversion (%)	Catalyst	TOS (min)		
54.8	0.5Zn/ZSM-5	10	63.0	22.4	26.4
		50	63.8	22.7	28.0
	ZSM-5 + 0.5Zn/ZSM-5	10	66.3	23.7	25.6
		50	65.9	22.7	26.3

3. Materials and Methods

3.1. Catalyst Preparation

NH_4 -ZSM-5 with Si/Al molar ratio of 15 (CBV 3024E, Zeolyst International, Whitmarsh, PA, USA) was commercially purchased. The NH_4 -ZSM-5 was passed through the calcination step at 550 °C for 6 h under air condition to further convert to protonated form. For abbreviation, protonated H-ZSM-5 will be designated as ZSM-5 throughout the text. Zn-impregnated ZSM-5 was prepared by solution impregnation method using appropriate concentration of aqueous solution of Zn nitrate hexahydrate ($Zn(NO_3)_2 \cdot 6H_2O$) (Wako, Chuo, Osaka, Japan). After the impregnation step, samples were dried at 110 °C overnight. Then, the calcination step at 550 °C for 6 h under air condition could finalize the catalyst. The impregnated zeolite was named $xZn/ZSM-5$, where x is the weight percentage of Zn.

3.2. Catalyst Characterization

To investigate the crystallinities of the samples, X-ray diffraction (XRD, MiniFlex II, Rigaku, Akishima, Tokyo, Japan) was conducted with Cu K α radiation with the scanning rate of 4 °/min ranging 3–90°. Scanning electron microscopy (SEM) and energy dispersive X-ray spectroscopy (EDS) analyses were performed to investigate the surface atomic distribution of the samples (JSM–6010LA, JEOL, Akishima, Tokyo, Japan). To obtain more accurate information of the distribution, high-resolution transmission electron microscope (HR–TEM) and EDS analyses (JEM–2100F, JEOL, Akishima, Tokyo, Japan) were operated. N₂ physisorption analysis was conducted for the characterization of pore volume and surface area of the samples by applying Brunauer–Emmett–Teller (BET) equation at –196 °C. Inductively coupled plasma optical emission spectroscopy (ICP–OES, iCAP 7000, Thermo Fisher, Waltham, MA, USA) was conducted to analyze Zn, Al, and Si contents in the samples. Typically, 50 mg of sample was dissolved in hydrofluoric acid and nitric acid. Then, the sample was diluted 50 times. The diluted samples were measured after calibration with atomic standard solution for Zn, Al, and Si. Temperature-programmed desorption of NH₃ (NH₃–TPD, BELCAT–M, Microtrac BEL, Suminoe, Osaka, Japan) was conducted to investigate the acidity of the samples. After the pretreatment step at 500 °C for 1 h under He flow, samples were cooled down to 100 °C and 3%NH₃/He gas was fed for 30 min for adsorption of NH₃. Then, weakly adsorbed NH₃ was desorbed under He flow at 100 °C for 15 min. The samples were then heated to 800 °C (10 °C/min) and concentration of desorbed NH₃ was detected by TCD detector. To investigate the species of incorporated Zn, X-ray photoelectron spectroscopy (XPS) was conducted using K–alpha (Thermo Fisher, Waltham, MA, USA) with an X-ray source of monochromated Al K α . For calibration, the spectra were acquired from Cu, Ag, and Au after sputtering to remove contamination. The peak position values were determined, and the energy scale recalibrated using the standard peak position for Cu2p 3/2, Ag 3d 5/2, Au 4f 7/2. For the analysis of the amount and species of coke deposited on the samples after each reaction, thermogravimetric analysis (TGA) was conducted with TGA4000 (Perkin Elmer, Waltham, MA, USA).

3.3. Catalytic Activity Tests

The mixture of saturated and unsaturated light hydrocarbons was used as feed gas. It was composed of 7.50% C₂H₂, 1.13% C₂H₄, 0.803% C₃H₈, 2.06% n-C₄H₁₀, 36.70% H₂, and 50.137% N₂ as shown in Table 1. This composition was based on the composition of effluent gas mixture from a low-temperature plasma reactor for methane conversion [15] and it was slightly modified for our study. The catalytic activity test was conducted at 700 °C and atmospheric pressure with 1/2 inch outer-diameter microfixed-bed quartz tubular reactor. A total of 0.2 g of zeolite was loaded in isothermal zone of the reactor and diluted with 0.6 g of 1 ϕ α -Al₂O₃ balls. The catalyst bed was heated to 700 °C at the ramping rate of 5 °C/min under N₂ flow. When the temperature reached the prescribed reaction temperature, the feed gas was fed to the catalyst bed at gas hourly space velocity (GHSV) of 20,000 mL/g_{cat}/h. Online gas chromatograph (GC) was utilized to analyze the effluent gases after the reaction. CH₄, C₂H₆, C₂H₄, C₂H₂, C₃H₈, C₃H₆, n-C₄H₁₀, benzene, toluene, xylenes, ethylbenzene, styrene, and naphthalene were analyzed by FID equipped with gaspro capillary column, and H₂ and internal standard N₂ were analyzed by TCD equipped with carboxen–1000 column. To prevent condensation of the aromatic compounds, lines were heated to 220 °C and carefully insulated. The catalytic aromatization reaction tests from ethane, ethylene, and acetylene as a sole hydrocarbon reactant were conducted by employing feed composition of C₂:H₂:N₂ = 1:2:7 and other conditions were maintained in the same manner as the previous case of aromatization from hydrocarbon mixture. Total carbon conversion, selectivity of products, and yield of products are calculated as follows, where F is molar flow rate and N^{carbon} is carbon number.

$$\text{Total carbon conversion} = \frac{\sum F_{\text{reactant}}^{\text{inlet}} N_{\text{reactant}}^{\text{carbon}} - \sum F_{\text{reactant}}^{\text{outlet}} N_{\text{reactant}}^{\text{carbon}}}{\sum F_{\text{reactant}}^{\text{inlet}} N_{\text{reactant}}^{\text{carbon}}} \quad (1)$$

$$\text{Selectivity of products} = \frac{F_{\text{product}}^{\text{outlet}} N_{\text{product}}^{\text{carbon}}}{\sum F_{\text{reactant}}^{\text{inlet}} N_{\text{reactant}}^{\text{carbon}} - \sum F_{\text{reactant}}^{\text{outlet}} N_{\text{reactant}}^{\text{carbon}}} \quad (2)$$

$$\text{Yield of products} = \frac{F_{\text{product}}^{\text{outlet}} N_{\text{product}}^{\text{carbon}}}{\sum F_{\text{reactant}}^{\text{inlet}} N_{\text{reactant}}^{\text{carbon}}} \quad (3)$$

4. Conclusions

The Zn-impregnated ZSM-5 catalysts were employed for conversion and aromatization of saturated and unsaturated light hydrocarbon mixture with hydrogen. Five different kinds of Zn-impregnated, unimpregnated, and physically mixed catalyst beds were tested to assess and improve total aromatics yield as well as BTX yield. The acidic properties of the ZSM-5 catalysts changed when Zn was incorporated. The impregnation of Zn led to the formation of medium acid sites, which were derived by the formation of $[\text{Zn}-\text{O}-\text{Zn}]^{2+}$ structure playing a role of Lewis acid site. However, the number of $[\text{Zn}-\text{O}-\text{Zn}]^{2+}$ sites decreased as the amount of Zn increased. It was found that 0.5Zn/ZSM-5 showed the highest aromatics yield, but it decreased as the amount of Zn loading was increased further. The physically mixed bed with Zn/ZSM-5 and unimpregnated ZSM-5 showed a slightly lower aromatics yield, whereas the BTX yield was found to be highest due to balanced distribution of acid-site species. It seemed that the $[\text{Zn}-\text{O}-\text{Zn}]^{2+}$ species identified and quantified in relative composition by XPS played a crucial role as a Lewis acid site and enhanced total aromatics yields. From the result with different feeds, the conversion of ethylene was found to be more significant than that of ethane and acetylene. In addition, we think that the feed mixture in this study had similar aspects of the natural gas liquids and the intermediate molecules in the middle of conversion processes from methane in terms of their compositions and kinds. Therefore, it is believed that the findings of this study could be applied and extended to conversions of NGL and intermediate hydrocarbon mixture to produce more value-added products.

Supplementary Materials: The following supporting information can be downloaded at: <https://www.mdpi.com/article/10.3390/catal12050501/s1>, Figure S1. XRD results of ZSM-5, 0.5Zn/ZSM-5, and 1Zn/ZSM-5; Figure S2. N_2 physisorption isotherm results of ZSM-5, 0.25Zn/ZSM-5, 0.5Zn/ZSM-5, and 1Zn/ZSM-5; Figure S3. Pore-size distribution of ZSM-5, 0.25Zn/ZSM-5, 0.5Zn/ZSM-5, and 1Zn/ZSM-5; Figure S4. Aliphatic hydrocarbons selectivity of A: ZSM-5, B: 0.5Zn/ZSM-5, C: 1Zn/ZSM-5, D: ZSM-5 + 0.5Zn/ZSM-5, and E: 0.25Zn/ZSM-5; Figure S5. TG/DTA results of spent (a) ZSM-5, (b) 0.5Zn/ZSM-5, (c) 1Zn/ZSM-5, (d) ZSM-5 + 0.5Zn/ZSM-5, and (e) 0.25Zn/ZSM-5; Table S1. Result of nonthermal plasma-assisted methane conversion.

Author Contributions: Investigation and writing, H.S.; experiment and analysis: J.H.; investigation and supervision: K.-S.H. All authors have read and agreed to the published version of the manuscript.

Funding: This work was financially supported by the Center for C1 Gas Refinery funded by Ministry of Science and ICT (NRF-2018M3D3A1A01018004), and also supported by the National Research Foundation of Korea (NRF-2019M3F4A1073044).

Data Availability Statement: Not applicable.

Conflicts of Interest: The authors declare no conflict of interest.

References

1. Borry, R.W.; Kim, Y.H.; Huffsmith, A.; Reimer, J.A.; Iglesia, E. Structure and Density of Mo and Acid Sites in Mo-Exchanged H-ZSM5 Catalysts for Nonoxidative Methane Conversion. *J. Phys. Chem. B* **1999**, *103*, 5787–5796. [[CrossRef](#)]
2. Ding, W.; Li, S.; Meitzner, G.D.; Iglesia, E. Methane Conversion to Aromatics on Mo/H-ZSM5: Structure of Molybdenum Species in Working Catalysts. *J. Phys. Chem. B* **2001**, *105*, 506–513. [[CrossRef](#)]
3. Liu, S.; Wang, L.; Ohnishi, R.; Ichikawa, M. Bifunctional Catalysis of Mo/HZSM-5 in the Dehydroaromatization of Methane to Benzene and Naphthalene XAFS/TG/DTA/MASS/FTIR Characterization and Supporting Effects. *J. Catal.* **1999**, *181*, 175–188. [[CrossRef](#)]

4. Tshabalala, T.E.; Coville, N.J.; Scurrrell, M.S. Dehydroaromatization of methane over doped Pt/Mo/H-ZSM-5 zeolite catalysts: The promotional effect of tin. *Appl. Catal. A Gen.* **2014**, *485*, 238–244. [[CrossRef](#)]
5. Farrell, B.L.; Igenegbai, V.O.; Linic, S. A Viewpoint on Direct Methane Conversion to Ethane and Ethylene Using Oxidative Coupling on Solid Catalysts. *ACS Catal.* **2016**, *6*, 4340–4346. [[CrossRef](#)]
6. Guo, X.; Fang, G.; Li, G.; Ma, H.; Fan, H.; Yu, L.; Ma, C.; Wu, X.; Deng, D.; Wei, M.; et al. Direct, Nonoxidative Conversion of Methane to Ethylene, Aromatics, and Hydrogen. *Science* **2014**, *344*, 616–619. [[CrossRef](#)]
7. Lim, T.H.; Kim, D.H. Characteristics of Mn/H-ZSM-5 catalysts for methane dehydroaromatization. *Appl. Catal. A Gen.* **2019**, *577*, 10–19. [[CrossRef](#)]
8. Gim, M.Y.; Han, S.J.; Kang, T.H.; Song, J.H.; Kim, T.H.; Kim, D.H.; Lee, K.-Y.; Song, I.K. Benzene, Toluene, and Xylene Production by Direct Dehydroaromatization of Methane Over WO₃/HZSM-5 Catalysts. *J. Nanosci. Nanotechnol.* **2017**, *17*, 8226–8231. [[CrossRef](#)]
9. Kim, J.; Abbott, M.S.; Go, D.B.; Hicks, J.C. Enhancing C–H Bond Activation of Methane via Temperature-Controlled, Catalyst–Plasma Interactions. *ACS Energ. Lett.* **2016**, *1*, 94–99. [[CrossRef](#)]
10. Kameshima, S.; Tamura, K.; Ishibashi, Y.; Nozaki, T. Pulsed dry methane reforming in Plasma—Enhanced catalytic reaction. *Catal. Today* **2015**, *256*, 67–75. [[CrossRef](#)]
11. Zheng, X.; Tan, S.; Dong, L.; Li, S.; Chen, H. Silica—Coated LaNiO₃ nanoparticles for non-thermal plasma assisted dry reforming of methane: Experimental and kinetic studies. *Chem. Eng. J.* **2015**, *265*, 147–156. [[CrossRef](#)]
12. Mahammadunnisa, S.; Reddy, P.M.K.; Ramaraju, B.; Subrahmanyam, C. Catalytic Nonthermal Plasma Reactor for Dry Reforming of Methane. *Energy Fuels* **2013**, *27*, 4441–4447. [[CrossRef](#)]
13. Zheng, X.-G.; Tan, S.-Y.; Dong, L.-C.; Li, S.-B.; Chen, H.-M.; Wei, S.-A. Experimental and kinetic investigation of the plasma catalytic dry reforming of methane over perovskite LaNiO₃ nanoparticles. *Fuel Process. Technol.* **2015**, *137*, 250–258. [[CrossRef](#)]
14. Zeng, Y.; Zhu, X.; Mei, D.; Ashford, B.; Tu, X. Plasma—Catalytic dry reforming of methane over γ -Al₂O₃ supported metal catalysts. *Catal. Today* **2015**, *256*, 80–87. [[CrossRef](#)]
15. Kim, J.; Jeoung, J.; Jeon, J.; Kim, J.; Mok, Y.S.; Ha, K.-S. Effects of dielectric particles on non-oxidative coupling of methane in a dielectric barrier discharge plasma reactor. *Chem. Eng. J.* **2019**, *377*, 119896. [[CrossRef](#)]
16. Ma, D.; Shu, Y.; Bao, X.; Xu, Y. Methane Dehydro—Aromatization under Nonoxidative Conditions over Mo/HZSM-5 Catalysts: EPR Study of the Mo Species on/in the HZSM-5 Zeolite. *J. Catal.* **2000**, *189*, 314–325. [[CrossRef](#)]
17. Raad, M.; Hamieh, S.; Toufaily, J.; Hamieh, T.; Pinard, L. Propane aromatization on hierarchical Ga/HZSM-5 catalysts. *J. Catal.* **2018**, *366*, 223–236. [[CrossRef](#)]
18. Tshabalala, T.E.; Scurrrell, M.S. Aromatization of *n*-hexane over Ga, Mo and Zn modified H-ZSM-5 zeolite catalysts. *Catal. Commun.* **2015**, *72*, 49–52. [[CrossRef](#)]
19. Ma, L.; Zou, X. Cooperative catalysis of metal and acid functions in Re-HZSM-5 catalysts for ethane dehydroaromatization. *Appl. Catal. B Environ.* **2019**, *243*, 703–710. [[CrossRef](#)]
20. Bhan, A.; Delgass, W.N. Propane Aromatization over HZSM-5 and Ga/HZSM-5 Catalysts. *Catal. Rev.* **2008**, *50*, 19–151. [[CrossRef](#)]
21. Nishi, K.; Komai, S.-i.; Inagaki, K.; Satsuma, A.; Hattori, T. Structure and catalytic properties of Ga-MFI in propane aromatization. *Appl. Catal. A Gen.* **2002**, *223*, 187–193. [[CrossRef](#)]
22. Rodrigues, V.d.O.; Júnior, A.C.F. On catalyst activation and reaction mechanisms in propane aromatization on Ga/HZSM5 catalysts. *Appl. Catal. A Gen.* **2012**, *435*, 68–77. [[CrossRef](#)]
23. Wang, J.; Kang, M.; Zhang, Z.; Wang, X. Propane Aromatization over Mo/HZSM-5 Catalysts. *J. Nat. Gas Chem.* **2002**, *11*, 43–50.
24. Solymosi, F.; Széchenyi, A. Aromatization of *n*-butane and 1-butene over supported Mo₂C catalyst. *J. Catal.* **2004**, *223*, 221–231. [[CrossRef](#)]
25. Mehdad, A.; Lobo, R.F. Ethane and ethylene aromatization on Zinc—Containing zeolites. *Catal. Sci. Technol.* **2017**, *7*, 3562–3572. [[CrossRef](#)]
26. Kazansky, V.B.; Subbotina, I.R.; Rane, N.; van Santen, R.A.; Hensen, E.J.M. On two alternative mechanisms of ethane activation over ZSM-5 zeolite modified by Zn²⁺ and Ga¹⁺ cations. *Phys. Chem. Chem. Phys.* **2005**, *7*, 3088–3092. [[CrossRef](#)]
27. Zhang, Y.; Wu, S.; Xu, X.; Jiang, H. Ethane aromatization and evolution of carbon deposits over nanosized and microsized Zn/ZSM-5 catalysts. *Catal. Sci. Technol.* **2020**, *10*, 835–843. [[CrossRef](#)]
28. Gong, Q.; Fang, T.; Xie, Y.; Zhang, R.; Liu, M.; Barzagli, F.; Li, J.; Hu, Z.; Zhu, Z. High-Efficiency Conversion of Methanol to BTX Aromatics Over a Zn-Modified Nanosheet-HZSM-5 Zeolite. *Ind. Eng. Chem. Res.* **2021**, *60*, 1633–1641. [[CrossRef](#)]
29. Zhang, G.Q.; Bai, T.; Chen, T.F.; Fan, W.T.; Zhang, X. Conversion of Methanol to Light Aromatics on Zn-Modified Nano-HZSM-5 Zeolite Catalysts. *Ind. Eng. Chem. Res.* **2014**, *53*, 14932–14940. [[CrossRef](#)]
30. Li, J.; Gong, Q.; Liu, Y.; Kang, R.; Yang, C.; Qiu, M.; Hu, Z.; Zhu, Z. Insight into the Formation of CO_x By-Products in Methanol-to-Aromatics Reaction over Zn/HZSM-5: Significantly Affected by the Chemical State of Surface Zn Species. *Chem. Cat. Chem.* **2019**, *11*, 4755–4764.
31. Hsieh, C.-Y.; Chen, Y.-Y.; Lin, Y.-C. Ga-Substituted Nanoscale HZSM-5 in Methanol Aromatization: The Cooperative Action of the Brønsted Acid and the Extra-Framework Ga Species. *Ind. Eng. Chem. Res.* **2018**, *57*, 7742–7751. [[CrossRef](#)]
32. Xin, Y.; Qi, P.; Duan, X.; Lin, H.; Yuan, Y. Enhanced Performance of Zn-Sn/HZSM-5 Catalyst for the Conversion of Methanol to Aromatics. *Catal. Lett.* **2013**, *143*, 798–806. [[CrossRef](#)]

33. Niu, X.; Gao, J.; Miao, Q.; Dong, M.; Wang, G.; Fan, W.; Qin, Z.; Wang, J. Influence of preparation method on the performance of Zn-containing HZSM-5 catalysts in methanol-to-aromatics. *Microporous Mesoporous Mater.* **2014**, *197*, 252–261. [[CrossRef](#)]
34. Niu, X.; Gao, J.; Wang, K.; Miao, Q.; Dong, M.; Wang, G.; Fan, W.; Qin, Z.; Wang, J. Influence of crystal size on the catalytic performance of H-ZSM-5 and Zn/H-ZSM-5 in the conversion of methanol to aromatics. *Fuel Process. Technol.* **2017**, *157*, 99–107. [[CrossRef](#)]
35. Bi, Y.; Wang, Y.; Chen, X.; Yu, Z.; Xu, L. Methanol aromatization over HZSM-5 catalysts modified with different zinc salts. *Chin. J. Catal.* **2014**, *35*, 1740–1751. [[CrossRef](#)]
36. Wang, J.; Li, W.; Hu, J. Study of methanol to aromatics on ZnHZSM-5 catalyst. *J. Fuel Chem. Technol.* **2009**, *37*, 607.
37. Su, X.; Zan, W.; Bai, X.; Wang, G.; Wu, W. Synthesis of microscale and nanoscale ZSM-5 zeolites: Effect of particle size and acidity of Zn modified ZSM-5 zeolites on aromatization performance. *Catal. Sci. Technol.* **2017**, *7*, 1943–1952. [[CrossRef](#)]
38. Klein, J.C.; Hercules, D.M. Surface characterization of model Urushibara catalysts. *J. Catal.* **1983**, *82*, 424–441. [[CrossRef](#)]
39. Guisnet, M.; Gnep, N. Aromatization of propane over GaHMFI catalysts. Reaction scheme, nature of the dehydrogenating species and mode of coke formation. *Catal. Today* **1996**, *31*, 275–292. [[CrossRef](#)]
40. Lee, W.; Lee, T.; Jang, H.-G.; Cho, S.J.; Choi, J.; Ha, K.-S. Effects of hierarchical zeolites on aromatization of acetylene. *Catal. Today* **2018**, *303*, 177–184. [[CrossRef](#)]
41. Lee, T.; Bae, Y.; Jeon, J.; Kim, J.; Choi, J.; Ha, K.-S. Effects of nanosheet catalysts on synthesis of aromatics and light hydrocarbons from acetylene. *Catal. Today* **2020**, *352*, 183–191. [[CrossRef](#)]
42. Song, C.; Gim, M.Y.; Lim, Y.H.; Kim, D.H. Enhanced yield of benzene, toluene, and xylene from the co-aromatization of methane and propane over gallium supported on mesoporous ZSM-5 and ZSM-11. *Fuel* **2019**, *251*, 404–412. [[CrossRef](#)]
43. le van Mao, R.; Yao, J. Kinetic study of n-butane aromatization on ZSM-5 and gallium bearing ZSM-5 catalysts. *Appl. Catal. A Gen.* **1991**, *79*, 77–87. [[CrossRef](#)]
44. Kazansky, V.B.; Pidko, E.A. Intensities of IR Stretching Bands as a Criterion of Polarization and Initial Chemical Activation of Adsorbed Molecules in Acid Catalysis. Ethane Adsorption and Dehydrogenation by Zinc Ions in ZnZSM-5 Zeolite. *J. Phys. Chem. B* **2005**, *109*, 2103–2108. [[CrossRef](#)]
45. Barbosa, L.A.M.M.; van Santen, R.A. Study of the Activation of C-H and H-H Chemical Bonds by the $[ZnOZn]^{2+}$ Oxyanion: Influence of the Zeolite Framework Geometry. *J. Phys. Chem. B* **2003**, *107*, 14342–14349. [[CrossRef](#)]
46. Hsu, Y.; Lee, T.; Hu, H. Isomerization of ethylbenzene and m-xylene on zeolites. *Ind. Eng. Chem. Res.* **1988**, *27*, 942–947. [[CrossRef](#)]
47. Namuangruk, S.; Pantu, P.; Limtrakul, J. Alkylation of benzene with ethylene over faujasite zeolite investigated by the ONIOM method. *J. Catal.* **2004**, *225*, 523–530. [[CrossRef](#)]
48. Young, L.; Butter, S.; Kaeding, W. Shape selective reactions with zeolite catalysts: III. Selectivity in xylene isomerization, toluene-methanol alkylation, and toluene disproportionation over ZSM-5 zeolite catalysts. *J. Catal.* **1982**, *76*, 418–432. [[CrossRef](#)]
49. Tsai, P.; Anderson, J. Reaction acetylene over ZSM-5-type catalysts. *J. Catal.* **1983**, *80*, 207–214. [[CrossRef](#)]